

# Aerosols: the key to understanding Titan's lower ionosphere

G.J. Molina-Cuberos<sup>a</sup>, S. Cardnell<sup>b</sup>, A.J. García-Collado<sup>c</sup>, O. Witasse<sup>b</sup>,  
J.J. López-Moreno<sup>d</sup>

<sup>a</sup>*Departamento de Electromagnetismo y Electrónica, Universidad de Murcia, Murcia, Spain.*

<sup>b</sup>*European Space Agency, ESA/ESTEC Scientific Support Office, Directorate of Science, Noordwijk, The Netherlands.*

<sup>c</sup>*Geomática, Teledetección y SIG Aplicados, Universidad Católica de San Antonio, Murcia, Spain.*

<sup>d</sup>*Instituto de Astrofísica de Andalucía, IAA-CSIC, Granada, Spain.*

---

## Abstract

The Permittivity Wave and Altimetry system on board the Huygens probe observed an ionospheric hidden layer at a much lower altitude than the main ionosphere during its descent through the atmosphere of Titan, the largest satellite of Saturn. Previous studies predicted a similar ionospheric layer. However, neither previous nor post-Huygens theoretical models have been able to reproduce the measurements of the electrical conductivity and charge densities reported by the Mutual Impedance (MI) and Relaxation Probe (RP) sensors. The measurements were made from an altitude of 140 km down to the ground and show a maximum of charge densities of  $\approx 2 \times 10^9 \text{ m}^{-3}$  positive ions and  $\approx 450 \times 10^6 \text{ m}^{-3}$  electrons at approximately 65 km. Such a large difference between positive and negative charge densities has not yet been understood. Here, by making use of electron and ion capture processes in to aerosols, we are able to model both electron and positive ion number densities and to reconcile experimental data and model results.

13 *Keywords:* Titan, Comic Rays, Aerosols, charge concentration, ionosphere

---

## 14 **1. Introduction**

15 The atmosphere and surface of Titan, the largest moon of **Saturn**, was  
16 explored by the ESA Huygens Probe in 2005 (*Lebreton et al.*, 2005). During  
17 the three hours of descent and surface operations, the probe measured for the  
18 very first time the physical properties of its deeper atmosphere and hidden  
19 surface. The Permittivity **Wave** and Altimetry (PWA) subsystem, part of  
20 the Huygens Atmospheric Structure Instrument (HASI), determined the at-  
21 mospheric electrical conductivity by making use of two independent sensors:  
22 the Mutual Impedance (MI) and Relaxation Probe (RP) and discovered an  
23 ionized layer at approximately 65 km of altitude (*Fulchignoni et al.*, 2005;  
24 *Grard et al.*, 2006).

25 This low ionospheric layer is **thought to be** produced by cosmic radiation  
26 (*Capone et al.*, 1976; *Molina-Cuberos et al.*, 1999b), which is the most pen-  
27 etrating kind of radiation and the only one able to ionize the lower portion  
28 of the atmosphere. Cosmic rays ionize the neutral constituents of the atmo-  
29 sphere, producing positive ions and electrons. The PWA data shows that,  
30 for example, at the peak of electron density, the concentration of positive  
31 ions is approximately four times higher than that of electrons, and the ratio  
32 increases with altitude, reaching a factor of approximately 1000 at the top  
33 of the sounding range, 140 km (*Hamelin et al.*, 2007; *López-Moreno et al.*,  
34 2008; *Molina-Cuberos et al.*, 2010). In order to explain dissimilar concen-  
35 trations of electrons and positive ions reported by the PWA sensors in the  
36 lower ionosphere, either electrophilic molecular species, embryos or aerosol

37 particles able to attain negative charge must be considered (*Borucki et al.*,  
38 2006, 2008; *Whitten et al.*, 2007; *Mishra et al.*, 2015).

39 The existence of an upper ionospheric layer was known since the Voy-  
40 ager 1 flyby (*Bird et al.*, 1997). This layer extends up to approximagely  
41 2200 km altitude (*Galand et al.*, 2014) and it is produced by ultraviolet ra-  
42 diation from the sun on the dayside (*Cravens et al.*, 2005) and energetic  
43 particle on the nightside(*Cravens et al.*, 2009). Electrons trapped in the  
44 Saturnian magnetosphere can also contribute to the ionization depending on  
45 the Saturnian magnetosphere and the Saturn Local time of Titan (*Edberg et*  
46 *al.*, 2015). The dayside electron number densities deduced from the Radio  
47 Plasma Wave Science/Langmuir Probe (RPWS/LP) measurements peak at  
48 values  $\sim 2000 - 5000 \text{ cm}^{-3}$  in the altitude range from 1000 to 1200 km (*Vi-*  
49 *gren et al.*, 2015), and it results a factor of  $\sim 2$  lower than the values derived  
50 in the Cassini multi-instrumental study by *Vigren et al.* (2013).

51 Titan is the satellite with the densest atmosphere in the Solar System  
52 and the only nitrogen-rich atmosphere aside from Earth's. Its atmosphere  
53 is mainly composed by nitrogen (97%) and methane ( $2.7 \pm 1\%$ ), and lodges  
54 trace amounts of a high variety of hydrocarbons such us ethane, diacety-  
55 lene, methylacetylene, acetylene, and cyanoacetylene (*Niemann et al.*, 2005;  
56 *Coustenis and Taylor*, 2008). The atmosphere is characterized by dis-  
57 tributed hazes of aerosol layers and the known Titan's orange haze at alti-  
58 tudes of around 500 km (*Israël et al.*, 2005; *Coates et al.*, 2009; *Lavvas et*  
59 *al.*, 2013). Solar radiation and energetic particles coming from the Saturnian  
60 magnetosphere dissociate  $\text{N}_2$  and  $\text{CH}_4$ , the major atmospheric constituents,  
61 into radicals and ions, which trigger a complex organic chemistry (*Cravens*

62 *et al.*, 2006; *Magee et al.*, 2009; *Mandt et al.*, 2012) and subsequently leads  
63 to the formation of aerosol particles (*Niemann et al.*, 2005; *Coates et al.*,  
64 2009; *Lavvas et al.*, 2013). Those particles can then become charged pos-  
65 itively or negatively. At higher altitudes, just below the main ionospheric  
66 peak above 950 km, negative and positive molecular ions and predominantly  
67 negative charged nm-sized grains have been detected (*Coates et al.*, 2007;  
68 *Waite et al.*, 2007; *Shebanits et al.*, 2013, 2016). Several articles have shown  
69 the significant role of physical aggregation and ion-neutral chemistry in the  
70 production of aerosols (*Sittler et al.*, 2009; *Lindgren et al.*, 2017; *Lavvas et*  
71 *al.*, 2013). It is now widely admitted that studying the ionosphere of Titan  
72 at all altitudes cannot be done without considering aerosols.

73 The models developed before the Huygens arrival predicted that the elec-  
74 tron and ion abundances can be affected by attachment to aerosols, during  
75 both nighttime and daytime (*Borucki et al.*, 1987, 2006). The post-Huygens  
76 models also included other species to decrease the concentration of electrons  
77 and to reproduce the observations. *Whitten et al.* (2007) developed a time-  
78 dependent model of the nightside ionosphere and found that the electrical  
79 charging of aerosol particles is negative and the formation of negative ions  
80 is of major importance at night. The presence of a very small abundance  
81 (in the range between  $10^{-13}$  and  $10^{-11}$  mole fraction) of electrophilic neutral  
82 species in which electrons can be attached by the three-body process and  
83 produce negative ions, can reduce appreciably the concentration of electrons  
84 below 40 km (*Molina-Cuberos et al.*, 2000).

85 *Borucki et al.* (2008) modeled the size and abundance distribution of  
86 aerosols by assuming a constant mass flux with altitude and using the re-

87 ported optical depth at the lower ionosphere by *Tomasko et al. (2005)* as a  
88 constraint. Then, the obtained profiles were used to calculate the electron  
89 and ion densities and conductivities for various solar UV photoelectron emis-  
90 sion thresholds, because of the Huygens' descent took place during daytime  
91 conditions, with a solar zenith angle of around  $40^\circ$ . The comparison with  
92 PWA observations indicated that photoemission of electrons cannot be an  
93 important source of ionization (*Borucki et al., 2008*), therefore the structure  
94 of the lower ionosphere does not depend on the solar local time. In order  
95 to find agreement with observation, they also find that both an additional  
96 population of aerosol embryos above 50 km and a very low mole fraction of  
97 electrophilic molecules at lower altitudes are needed. Embryos are very small  
98 particles ( $\approx 7 \times 10^{-4} \mu\text{m}$ ) that, at the atmospheric conditions of Titan, can  
99 be fullerenes and polycyclic aromatic hydrocarbons (*Sittler et al., 2009*).

100 *Mishra et al. (2015)* solved the state equations for ions and electrons in  
101 the presence of aerosols and embryos, allowing both particles to be positively  
102 and negatively charged. In order to agree with the observations obtained  
103 by the MI sensor (*Hamelin et al., 2007*), both the concentration of embryos  
104 and the photoemission thresholds of aerosols/embryos were adjusted at each  
105 altitude. In contrast with *Borucki et al. (2008)*, the presence of aerosols  
106 increases the conductivity due to electrons and their predictions at 140 km  
107 differ approximately by four orders of magnitude with conductivity data  
108 retrieved from the RP sensor (*López-Moreno et al., 2008; Molina-Cuberos et*  
109 *al., 2010*).

110 In the present work, we take a step forward towards understanding the  
111 physical process related with the charge distribution in Titan's atmosphere

112 below 140 km. *Cardnell et al.* (2016) recently revealed the fundamental role  
113 that aerosols play in the photochemistry of the low ionosphere of Mars. Here  
114 we follow a similar approach and find that the size and density distribution  
115 of aerosols affects the concentration of both positive and negative charge car-  
116 riers. By making use of electron and ion capture processes onto aerosols and  
117 aerosol profiles from Huygens measurements (*Tomasko et al.*, 2008; *Lavvas*  
118 *et al.*, 2010), we are able to reconcile experimental data and model results.  
119 We also find that, unlike previous works, no additional population of small  
120 embryo particles nor electrophilic neutrals are needed in order to attain a  
121 reasonable agreement with the PWA observations.

## 122 **2. Model**

123 The lower ionosphere of Titan is modeled by considering the balance  
124 equations for one kind of cations, electrons and aerosols. A similar treatment  
125 was used by *Cardnell et al.* (2016) in the lower Martian ionosphere. Here we  
126 make use of the same processes and formulation with the only difference being  
127 neglecting electron photodetachment processes (*Borucki et al.*, 2008) due to  
128 the large distance to the Sun and the strong absorption of Titan's dense  
129 atmosphere (*Lara et al.*, 1996). The photoemission of aerosols was taken into  
130 account by *Mishra et al.* (2015) and they found that, in contrast with *Borucki*  
131 *et al.* (2008), the production of electrons by the photoemission of aerosols is  
132 an important process, particularly above 80 km. However, the inclusion of  
133 this process increases the concentration of electrons and the obtained results  
134 disagree with the observations above 80 km.

135 Transport phenomena can be neglected in the lower atmosphere because

136 the transport time is several orders of magnitude larger than the chemical  
 137 lifetime (*Molina-Cuberos et al.*, 1999a). Ions and electrons are produced  
 138 by cosmic rays and lost by ion-electron recombination and by attachment  
 139 to aerosols. Assuming steady-state conditions, the continuity equations for  
 140 positive ions, electrons and aerosols can be written as (*Banks and Kockarts*,  
 141 1973):

$$q - \alpha n^+ n^e - \sum_{i=-i_{max}}^{i_{max}-1} \beta_+^i n^+ N^i = 0 \quad (1)$$

$$q - \alpha n^+ n^e - \sum_{i=-i_{max}+1}^{i_{max}} \beta_e^i n^e N^i = 0 \quad (2)$$

$$\beta_+^{i-1} n^+ N^{i-1} + \beta_e^{i+1} n^e N^{i+1} - \beta_+^i n^+ N^i - \beta_e^i n^e N^i = 0 \quad (3)$$

142 where  $n^+$  and  $n^e$  are the cation and electron number densities, respectively,  
 143  $N^i$  is the number density of aerosols with  $i$  elementary charges,  $q$  is the  
 144 production rate of cations and electrons due to cosmic rays,  $\alpha$  the ion-electron  
 145 recombination coefficient,  $\beta_+^i$  and  $\beta_e^i$  are the attachment coefficients of cations  
 146 and electrons, respectively, to aerosols with  $i$  elementary charges, and  $\pm i_{max}$   
 147 is the maximum number of elementary charges in an aerosol.

148 We make use of the atmospheric model reported by *Coustenis and Taylor*  
 149 (2008) and an adapted cosmic rays spectra for Saturn's orbit and moderate  
 150 solar activity (*Molina-Cuberos et al.*, 1999b) in order to calculate the ion-  
 151 ization rate by cosmic rays. **Solar wind interacts with the cosmic particles**  
 152 **in the interplanetary medium and its variations related to the solar activity**  
 153 **produce changes in the spectrum of cosmic rays. However, due to the long**  
 154 **distance to the Sun and the strong absorption of the atmosphere,** the effects  
 155 of the solar conditions on the ionization rate below  $\approx 150$  km are quite low

156 (*Molina-Cuberos et al.*, 1999b), and, therefore, the results of our model do  
 157 not depend on the solar activity. The high amount of hydrocarbons and the  
 158 low temperatures of the atmosphere favour the production of cluster ions  
 159 (*Capone et al.*, 1976; *Borucki et al.*, 1987; *Molina-Cuberos et al.*, 1999a),  
 160 which are composed of the electrostatic aggregation of one or several neu-  
 161 tral molecules into an ion and recombine with electrons more quickly than  
 162 the covalently bonded cations. The ion-electron dissociative recombination  
 163 rates for the most abundant ions are on the form  $\alpha_{300} \times (T_e/300)^\gamma$ , with  $\alpha_{300}$   
 164 being the rate coefficient at  $T_e = 300$  K and with  $(T_e/300)^\gamma$  describing the  
 165 electron temperature dependence of the reaction (*Vigren et al.*, 2013). At  
 166 the lower atmosphere of Titan, the electron temperature is equal to the  
 167 atmospheric temperature,  $T$ . Experimental values for  $\alpha_{300}$  and  $\gamma$  range from  
 168 1 to 2 (in  $\times 10^{-6}$  cm<sup>3</sup> s<sup>-1</sup>) and from 0.58 to 0.80, respectively (see *Vigren*  
 169 *et al.* (2013) and references therein), here we have adopted a mean rate of  
 170  $\alpha = 1.5 \times 10^{-6} (300/T)^{0.7}$  cm<sup>3</sup> s<sup>-1</sup>.

171 Aerosols can become charged due to ion and electron attachment, both  
 172 positively and negatively up to several elementary charges. The more neg-  
 173 atively charged an aerosol is, the easier it is to capture a positive ion and  
 174 vice versa. The probability of electrons becoming attached to aerosols is  
 175 quantified with the electron attachment coefficient *Gunn* (1954):

$$\beta_e^i = \frac{i\mu_e e}{\epsilon_0(1 - \exp(-2L))} \quad (4)$$

176 where  $i$  is the number of charges on the aerosol,  $\mu_e$  the electron mobility,  $e$  is  
 177 the elementary charge,  $\epsilon_0$  is the vacuum permittivity,  $L = e^2/(8\pi\epsilon_0 a k_B T)$ ,  $a$   
 178 is the aerosol radius, and  $k_B$  is the Boltzmann constant. *Gunn* (1954) derived  
 179 the above expression by considering the Coulomb forces at large separations



180 between a spherical particle carrying  $i$  charges and the electron or ion, and  
181 by neglecting the induced image charges, which produce short range forces.  
182 Since the ionic mean free path is short compared to the aerosol size, we  
183 also make use of the method by *Gunn* (1954) to model the ion attachment  
184 to aerosol particles. This approximation is not applicable within the low  
185 collisional regime of the upper ionosphere. Aerosols are allowed to become  
186 charged up to  $\pm i_{max}$  elementary charges, which give rise to  $2i_{max} + 1$  aerosol  
187 balance equations. The maximum positive and negative charge the aerosols  
188 are allowed to attain is set at  $i_{max} = 150$ , which was twice the minimum  
189 value required to adequately represent the aerosol charge distribution.

190 The distribution of aerosols strongly affects the density of positive ions  
191 and electrons. In the present work, the two aerosol density profiles reported  
192 by *Tomasko et al.* (2008), with a constant aerosol size of  $720 \mu\text{m}$ , where  
193 used, see Fig. 1. These profiles were obtained using measurements from  
194 the two channels of the solar aureole (SA) instrument onboard Huygens,  
195 corresponding to the 491 and 934 nm wavelengths (*Tomasko et al.*, 2008).  
196 The results agree above 80 km, but differ slightly below this altitude. More  
197 recently, *Lavvas et al.* (2010) presented a one dimension study of Titan's  
198 aerosol distribution. They considered a constant mass production of aerosols  
199 in the thermosphere to  $3 \times 10^{-14} \text{g cm}^{-2} \text{s}^{-1}$  and modelled the evolution of the  
200 particles due to coagulation, sedimentation and atmospheric mixing. *Lavvas*  
201 *et al.* (2010) obtained a lower number density and an aerosol size of  $850 \mu\text{m}$ ,  
202 that can be considered constant at the altitude range of Huygens, also plotted  
203 in Fig. 1.

204 The aerosol charging processes do not alter the total aerosols number

205 density,  $N$ :

$$N = \sum_{i=-i_{max}}^{i_{max}} N^i \quad (5)$$

206 The condition of charge neutrality requires that:

$$\sum_{i=-i_{max}}^{i_{max}} iN^i + n^+ - n^e = 0 \quad (6)$$

207 The concentration of cations, electrons and charged aerosols were cal-  
208 culated by solving the system of algebraic equations (1)-(5), and using the  
209 *fsolve* function provided by Matlab<sup>TM</sup>. This technique iteratively minimizes  
210 the sum of squares of the components from an initial guess and a range of  
211 initial guess values were tested to ensure the final results. Once the charge  
212 concentrations are calculated, the mobilities due to positive ions and elec-  
213 trons are used to calculate the two branches of electrical conductivity, cor-  
214 responding to the positive and negative charges. Assuming that electrons  
215 mainly collide with molecular nitrogen, **the electron mobility can be derived**  
216 **as follows (*Banks and Kockarts, 1973*):**

$$\mu^e = \frac{e}{2.33 \times 10^{-17} N_n T} \quad (7)$$

217 where  $\mu^e$  is given in  $\text{m}^2 \text{s}^{-1} \text{V}^{-1}$  and  $N_n$  the neutral number density in  
218  $\text{m}^{-3}$ . The ionic mobility depends on the ionic mass. Here we make use of a  
219 functional equation (*Meyerott et al., 1980*):

$$\mu^+ = \frac{T}{273} \frac{101325}{P} \left[ \left( \frac{850}{m^+} \right)^{1/3} - 0.3 \right] \cdot 10^{-4} \quad (8)$$

220 where  $P$  the pressure in Pa and the ionic mass  $m^+$  is expressed in amu.  
221 Numerical models predict a mean ionic mass in the range between 50 and

222 150 amu (*Molina-Cuberos et al.*, 1999a), although more massive ions are not  
223 excluded. Here, we make use of a mean value of  $m^+ = 100$  amu.

### 224 **3. Results and Discussion**

225 Figure 2 compares the two components of the electrical conductivity re-  
226 sults with our model and the measurements obtained from the RP and MI  
227 data. The RP technique allows differentiation between the conductivity  
228 due to positive and negative charges and, therefore, can provide informa-  
229 tion about the densities of both charge carriers (*López-Moreno et al.*, 2008;  
230 *Molina-Cuberos et al.*, 2010). However, this method requires long time peri-  
231 ods, which decreases the spatial resolution. In contrast, the MI technique is  
232 only sensitive to the total electrical conductivity and has a faster measure-  
233 ment rate (*Hamelin et al.*, 2007).

234 The RP provided the conductivity due to positive ions above approx-  
235 imately 65 km; below this altitude the relaxation time was too long to be  
236 measured (*López-Moreno et al.*, 2008). We observe that the calculated con-  
237 ductivities are very similar for the three analyzed aerosol profiles. We have  
238 found a very good agreement with experimental results and does not differ  
239 too much from the results of the model not considering aerosols (also plotted  
240 in Fig 2).

241 The most important improvement of this model is the resulting conduc-  
242 tivity due to electrons. Without taking into account the role of aerosols  
243 (non-aerosol case in Fig 2), the results show a very good agreement below  
244 the peak at approximately 60 km. However, above this maximum, while  
245 the non-aerosol model predicts an increase in conductivity with altitude, the

246 measurements indicate an exponential decrease, reaching a disagreement of  
247 four orders of magnitude at 140 km. We observe that the inclusion of aerosols  
248 in the model strongly reduces the conductivity due to electrons, mainly at  
249 higher altitudes, and allows the convergence between model results and ex-  
250 perimental measurements. The best agreement is found with the aerosol  
251 profile retrieved from the 930 nm channel, in fact, calculations also reproduce  
252 the observed small decrease at around 80 km. MI reported conductivity mea-  
253 surements down to the ground (*Hamelin et al.*, 2007). However, the authors  
254 intentionally limited the density profile to an altitude of 40 km because of  
255 the lack of accuracy as the conductivity decreases. Our results also agree  
256 with the MI data, even at this altitude range, which may also support the  
257 measurements obtained by MI.

258 Figure 3 shows the densities of positive ions and electrons obtained by  
259 our model and the retrieved ones from the RP and MI measurements. The  
260 electron density, which obviously coincides with the positive ion density for  
261 the non-aerosol case, is also plotted. The error bars associated with the  
262 concentration of positive ions take into account the errors in the numerical  
263 fitting and the uncertainties of the ionic mass (*López-Moreno et al.*, 2008).  
264 Again, we observe a very good agreement between model predictions and the  
265 densities obtained from conductivity measurements. The presence of aerosols  
266 reduces the concentration of both electrons and ions. The decrease in the  
267 concentration of electrons is much greater and, therefore, the concentration  
268 of electrons is not equal to that of positive ions, which means that an im-  
269 portant amount of negative charge is accumulated on aerosols (Fig 4). In  
270 fact, the amount of negative charge attached onto aerosols is similar to the

271 number of electrons. The ratio ions/electrons decreases with altitude, from  
272 approximately 350 at the top of our altitude range to a minimum of approxi-  
273 mately 1.1 at  $\approx 70$  km, then it remains almost constant down to the ground,  
274 where the concentration of positive charge is twice that of electrons. Both  
275 electrons and positive ions peak at approximately 62 km, roughly the same  
276 altitude where ionization rate peaks (65 km).

277 Figure 4 shows the distribution of charged aerosols obtained in our sim-  
278 ulation. Aerosols tend to become negatively charged due to the more effi-  
279 cient attachment of electrons than that of positive ions. The mean num-  
280 ber of electrons attached to aerosol particles depends on altitude and is in  
281 the range between 30 and 50. Electron trapping in aerosols leads to  $\approx$   
282 60 charges/radius (in  $\mu\text{m}$ ), which is between the results obtained in tholin  
283 material, 628 charges/radius for Titan-like aerosols particles by *Pirim et al.*  
284 (2015) and the 7.5 charges/radius used by *Larson et al.* (2014) in a three di-  
285 mensional general circulation model with microphysics treatment of aerosols.  
286 At the maximum of the electron concentration, approximately 60 km, aerosol  
287 particles lodge approximately 30 electrons and close to the surface slightly  
288 more, approximately 35 electrons. The charged aerosol number density in-  
289 creases with altitude from the ground up to approximately 40 km, where it  
290 peaks at approximately  $1.4 \times 10^6 \text{ m}^{-3}$  and then decreases.

#### 291 4. Conclusions

292 The lower ionosphere of Titan has been modeled and the electrical con-  
293 ductivity due to positive charges and electrons was calculated in order to  
294 reconcile the experimental data obtained by the PWA system on board the

295 Huygens probe. The main conclusions obtained in this work are as follows:

296 1. The presence of aerosols reduces the values of the two components of  
297 the electrical conductivity. The used aerosol profile allows to reconcile the  
298 model results with the experimental measurements obtained both by the MI  
299 and the RP sensors in the whole altitude range, from 140 km down to the  
300 ground.

301 2. The inclusion of aerosols decreases the concentration of both electrons  
302 and ions. This reduction is greater for the case of electrons and, therefore,  
303 the concentration of electrons is not equal to that of positive ions. The ratio  
304 ions/electrons decreases with altitude, from  $\approx 350$  at 140 km to a minimum  
305 of  $\approx 1.1$  at  $\approx 70$  km.

306 3. Both electrons and positive ions peak at  $\approx 62$  km, roughly the same  
307 altitude where ionization rate peaks (65 km).

308 4. Aerosols are **negatively charged** and the main number of electrons  
309 attached to aerosol particles is in the range between 30 and 50.

## 310 **Acknowledgments**

311 The authors thank Panayotis Lavvas for his suggestions and comments.  
312 This work was supported by the Spanish Government (Project TEC2014-  
313 55463-C3-1-P) and by the European Commission (ERDF). O. Witasse and  
314 S. Cardnell acknowledge the ESA Young Graduate Trainee program.

## 315 **References**

316 Banks, P. M., and Kockarts, G. (1973), *Aeronomy, vol. 2* Academic Press,  
317 New York.

- 318 Bird, M. K., Dutta-Roy, R., Asmar, S. W., et al. (1997), Detection of Titan's  
319 Ionosphere from Voyager 1 Radio Occultation Observations, *Icarus* 130(2),  
320 426–436.
- 321 Borucki, W. J., Levin, Z., Whitten, R. C., et al (1987), Predictions of the  
322 electrical conductivity and charging of the aerosols in Titan's atmosphere,  
323 *Icarus* 72, 604 – 622.
- 324 Borucki, W. J., Whitten, R. C., Bakes, E. L. O., et al. (2006), Predictions  
325 of the electrical conductivity and charging of the aerosols in Titan's atmo-  
326 sphere, *Icarus* 181, 527 –544.
- 327 Borucki, W. J., and Whitten, R. C. (2008), Influence of high abundances of  
328 aerosols on the electrical conductivity of the Titan atmosphere, *Planetary  
329 and Space Sci.* 56, 19 –26.
- 330 Capone, L. A., Whitten, R. C., Dubach, J., Prasad, S. S., and Huntress,  
331 W. T., Jr. (1976), The lower ionosphere of Titan, *Icarus* 28, 367 –378.
- 332 Cardnell, S., Witasse, O., Molina-Cuberos, G. J., et al. (2016), A photochem-  
333 ical model of the dust-loaded ionosphere of Mars, *Journal of Geophysical  
334 Research (Planets)* 121, 2335 –2348.
- 335 Coates, A. J., Crary, F. J., Lewis, G. R., et al. (2007), Discovery of heavy  
336 negative ions in Titans ionosphere, *Geophys. Res. Lett.* 34(22), L22103.
- 337 Coates, A. J., Wellbrock, A., Lewis, G. R., et al. (2009), Heavy negative ions  
338 in Titan's ionosphere: Altitude and latitude dependence, *Planet. Space  
339 Sci.* 57(14-15), 1866–1871.

- 340 Cravens, T. E., Robertson, I. P., Clark, J., et al. (2005), Titan’s ionosphere:  
341 Model comparisons with Cassini Ta data, *Geophys. Res. Lett.* *32(12)*,  
342 L12108.
- 343 Cravens, T. E., Robertson, I. P., Waite, J. H., et al. (2006), Composition of  
344 Titan’s ionosphere, *Geophys. Res. Lett.* *33(7)*, L07105.
- 345 Cravens, T. E., Robertson, I. P., Waite, J. H., et al. (2009), Model-data  
346 comparisons for Titans nightside ionosphere, *Icarus* *199(1)*, 174188.
- 347 Coustenis, A., and Taylor, F. W. (2008), *Titan: Exploring an Earthlike*  
348 *World*, World Scientific, Singapore.
- 349 Edberg, N. J. T., Andrews, D. J., Bertucci, C., et al. (2015), Effects of  
350 Saturn’s magnetospheric dynamics on Titan’s ionosphere, *J. Geophys. Res.*  
351 *Sp. Phys.* *120(10)*, 8884-8898.
- 352 Fulchignoni, M., Ferri, F., Angrilli, F., et al. (2005), In situ measurements of  
353 the physical characteristics of Titan’s environment, *Nature* *438*, 785 –791.
- 354 Galand, M., Coates, A. J., Cravens, T. E., et al. (2014), Titan’s ionosphere,  
355 in *Titan*, edited by Muller-Wodarg, I., Griffith, C. A., Lellouch, E., and  
356 Cravens, T. E., 376–418, Cambridge University Press, Cambridge.
- 357 Grard, R., Hamelin, M., López-Moreno, J. J., et al. (2006), Electric proper-  
358 ties and related physical characteristics of the atmosphere and surface of  
359 Titan, *Planetary and Space Science* *54*, 1124 –1136.
- 360 Gunn, R. (1954), Diffusion charging of atmospheric droplets by ions, and the



- 361 resulting combination coefficients, *Journal of Atmospheric Sciences* 11(5)  
362 339–347.
- 363 Hamelin, M., Béghin, C., Grard, R., et al. (2007), Electron conductivity and  
364 density profiles derived from the mutual impedance probe measurements  
365 performed during the descent of Huygens through the atmosphere of Titan,  
366 *Planetary and Space Science* 55, 1964–1977.
- 367 Israël, G., Szopa, C., Raulin, F., et al. (2005), Complex organic matter in  
368 Titan’s atmospheric aerosols from in situ pyrolysis and analysis, *Nature*  
369 438, 796–799.
- 370 Lavvas, P., Yelle, R. V., and Griffith, C. A. (2010), Titans vertical aerosol  
371 structure at the Huygens landing site: Constraints on particle size, density,  
372 charge, and refractive index, *Icarus* 210, 832–842.
- 373 Lavvas, P., Yelle, R. V., Koskinen, T. et al. (2013), Aerosol growth in Titans  
374 ionosphere, *Proc Natl Acad Sci USA* 110,, no. 8, 2729–2734.
- 375 Lara, L. M., Lellouch, E., López-Moreno, J. J., et al. (1996), *Journal Geo-*  
376 *phys. Res.* 101, 23261.
- 377 Larson, E., Owen, T. B., and Friedson, J. A., (2014), Simulating Titans  
378 aerosols in a three dimensional general circulation model, *Icarus* 243, 400  
379 – 419.
- 380 Lebreton, J.-P., Witasse, O., Sollazzo, C., et al. (2005), An overview of the  
381 descent and landing of the Huygens probe on Titan, *Nature* 438, 758–764.

- 382 Lindgren, E. B., Stamm B., Chan H.-K., et al. (2017), The effect of like-  
383 charge attraction on aerosol growth in the atmosphere of Titan, *Icarus*  
384 *291*, 245–253.
- 385 López-Moreno, J. J., Molina-Cuberos, G. J., Hamelin, M., et al. (2008),  
386 Structure of Titan’s low altitude ionized layer from the Relaxation Probe  
387 onboard HUYGENS, *Geophysical Research Letters* *35*, L22104.
- 388 Magee, B. A., Waite, J. H., Mandt, K. E., et al. (2009), INMS-derived com-  
389 position of Titan’s upper atmosphere: Analysis methods and model com-  
390 parison, *Planet. Space Sci.* *57(14-15)*, 1895–1916.
- 391 Mandt, K. E., Gell, D. A., Perry, M., et al. (2012), Ion densities and compo-  
392 sition of Titan’s upper atmosphere derived from the Cassini Ion Neutral  
393 Mass Spectrometer: Analysis methods and comparison of measured ion  
394 densities to photochemical model simulations, *J. Geophys. Res.* *117(E10)*,  
395 E10006.
- 396 Meyerott, R. E., Reagan, J. B., and Joiner, R. G. (1980), The mobility and  
397 concentration of ions and the ionic conductivity in the lower stratosphere,  
398 *Journal of Geophysical Research* *85*, 1273 –1278.
- 399 Mishra, A., Michael, M., Tripathi, S. N., and Béghin, C. (2014), Revisited  
400 modeling of Titan’s middle atmosphere electrical conductivity, *Icarus* *238*,  
401 230 –234.
- 402 Molina-Cuberos, G. J., López-Moreno, J. J., Rodrigo, R., and Lara, L. M.  
403 (1999a), Chemistry of the galactic cosmic ray induced ionosphere of Titan,  
404 *Journal of Geophysical Research* *104*, 21997 –22024.

- 405 Molina-Cuberos, G. J., López-Moreno, J. J., Rodrigo, R., Lara, L. M., and  
406 O'Brien, K. (1999b), Ionization by cosmic rays of the atmosphere of Titan,  
407 *Planetary and Space Science* 47, 1347–1354.
- 408 Molina-Cuberos, G. J., López-Moreno, and J. J., Rodrigo (2000), Influence  
409 of Electrophilic Species on the Lower Ionosphere of Titan, *Geophysical*  
410 *Research Letters* 27 (9) 1351–1354.
- 411 Molina-Cuberos, G. J., Godard, R., López-Moreno, J. J., et al. (2010), A  
412 new approach for estimating Titan's electron conductivity based on data  
413 from relaxation probe sensors on the Huygens experiment, *Planetary and*  
414 *Space Science* 58, 1945–1952.
- 415 Niemann, H. B., Atreya, S. K., Bauer, S. J., et al (2005), The abundances  
416 of constituents of Titan's atmosphere from the GCMS instrument on the  
417 Huygens probe, *Nature* 438(7069), 779–784.
- 418 Pirim, C., Gann, R. D., McLain, J. L., et al. (2015), Electron-molecule chem-  
419 istry and charging processes on organic ices and Titan's icy aerosol surro-  
420 gates, *Icarus* 258, 109 – 119.
- 421 Shebanits, O., Wahlund, J.-E., K. Mandt, K., et al. (2013), Negative ion den-  
422 sities in the ionosphere of TitanCassini RPWS/LP results, *Planet. Space*  
423 *Sci.* 84, 153–162.
- 424 Shebanits, O., Wahlund, J.-E., Edberg, N. J. T., et al. (2016), *J. of Geophys.*  
425 *Res (Space Physics)* 121, 10.
- 426 Sittler, E. C., Ali, A., Cooper, J. F., et al. (2009), Heavy ion formation

- 427 in Titan's ionosphere: Magnetospheric introduction of free oxygen and a  
428 source of Titan's aerosols?, *Planetary and Space Science* 57, 1547–1557.
- 429 Tomasko, M. G., Archinal, B., Becker, T., et al. (2005), Rain, winds and  
430 haze during the Huygens probe's descent to Titan's surface, *Nature* 438,  
431 765–778.
- 432 Tomasko, M. G., Doose, L., Engel, S., et al. (2008), A model of Titan's  
433 aerosols based on measurements made inside the atmosphere, *Planetary  
434 and Space Science* 56, 669–707.
- 435 Vigren, E., Galand, M., Yelle, R.V., et al., (2013), On the thermal electron  
436 balance in Titan's sunlit upper atmosphere. *Icarus* 223, 234–251.
- 437 Vigren, E., Galand, M., Yelle, R. V., et al., (2015), Ionization balance in  
438 Titan's nightside ionosphere, *Icarus* 248, 539–546.
- 439 Waite, J. H., Young, D. T., Cravens, T. E., et al.(2007), The process of tholin  
440 formation in Titan's upper atmosphere, *Science* 316(5826), 870–875.
- 441 Whitten, R. C., Borucki, W. J., Tripath, S. (2007), Predictions of the electri-  
442 cal conductivity and charging of aerosols in Titan's nighttime atmosphere,  
443 *Journal of Geophysical Research* 112, E04001.

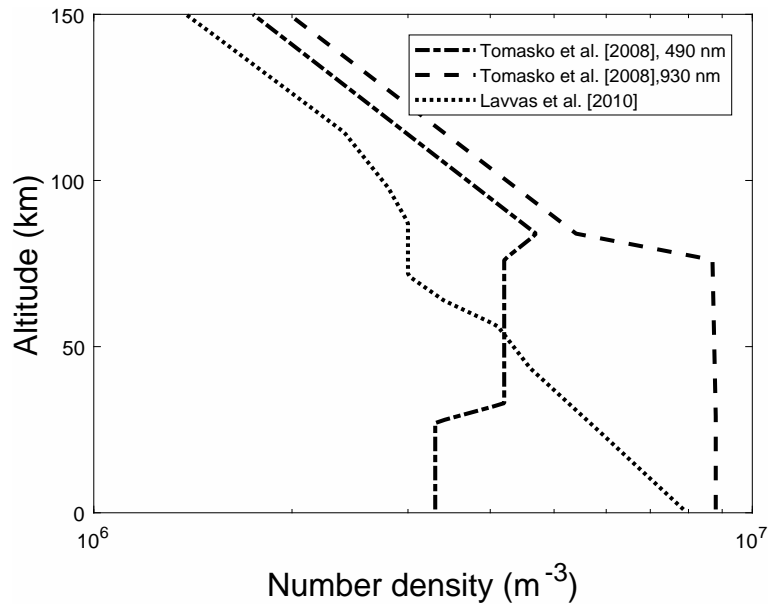


Figure 1: Aerosol number density as a function of altitude for the three different models used in this paper. All the models were developed for the Titan conditions during the descent of Huygens, same as the present model.

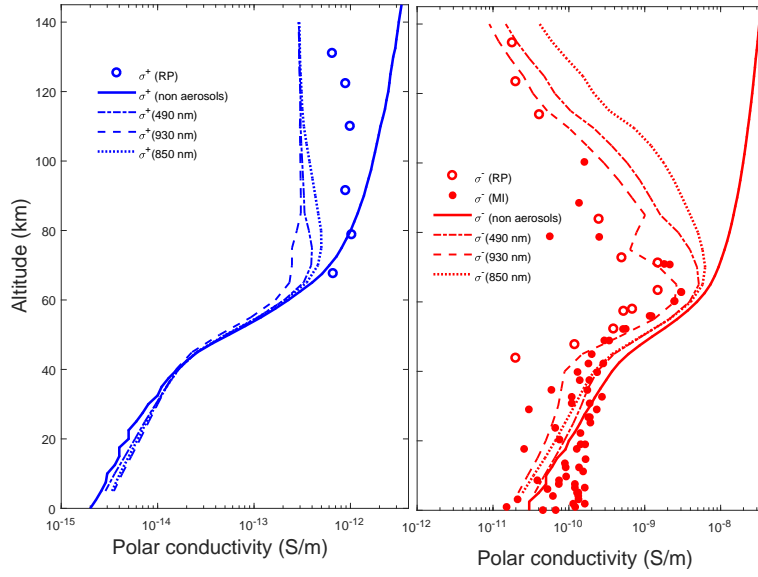


Figure 2: Electrical conductivity due to positive (left panel) and negative charges (right panel), where the symbols are for MI and RP measurements (*Hamelin et al.*, 2007; *López-Moreno et al.*, 2008; *Molina-Cuberos et al.*, 2010), solid line for the non-aerosol case and the other lines for the aerosol number densities shown in Fig. 1.

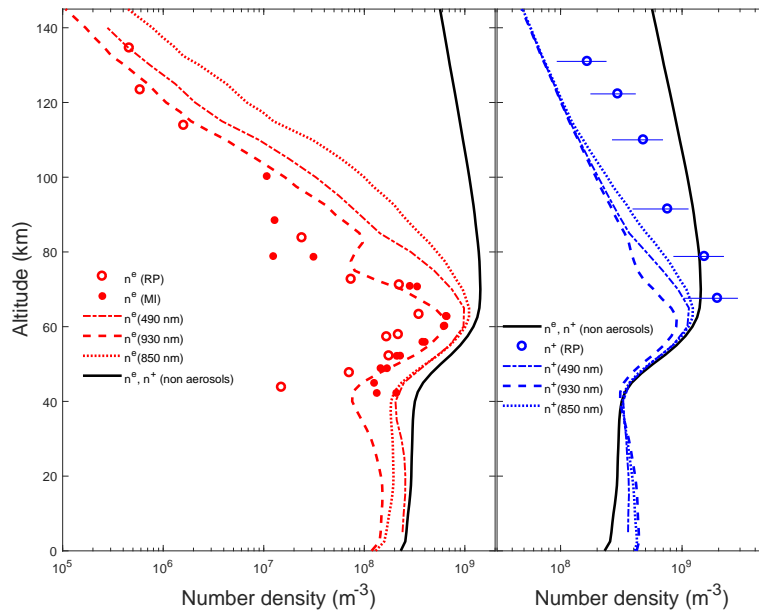


Figure 3: Calculated electron (left panel) and ion (right panel) densities (lines) and retrieved from MI and RP measurements (symbols).

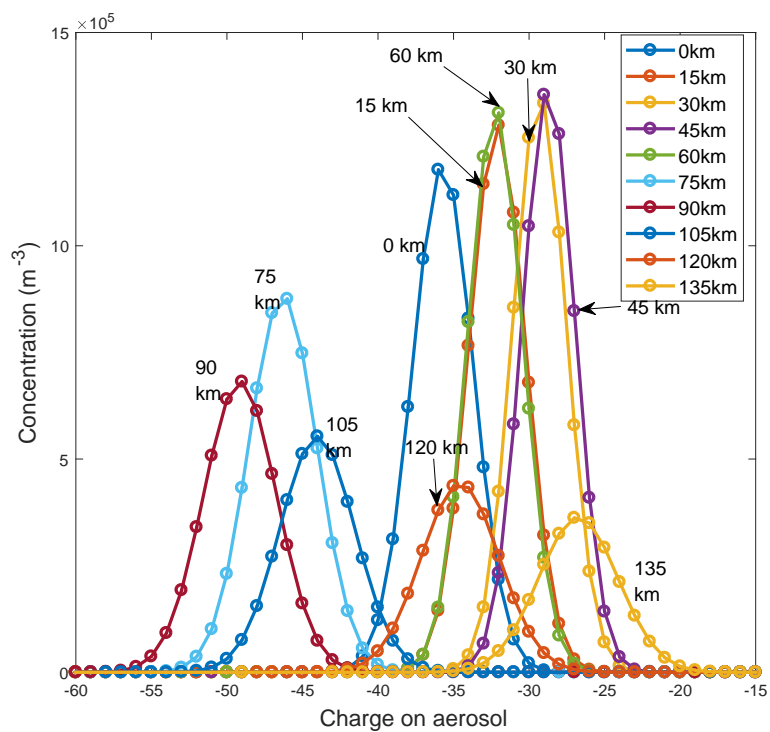


Figure 4: Distribution of charges on aerosols at various altitudes, the aerosol number density profile is from *Tomasko et al.* (2008) 930 nm, Fig. 1.